JACS
JOURNAL OF THE AMERICAN CHEMICAL SOCIETY
Article
pubs.acs.org/JACS

Nature-Inspired, Highly Durable CO_2 Reduction System Consisting of a Binuclear Ruthenium(II) Complex and an Organic Semiconductor Using Visible Light

Ryo Kuriki,[†] Hironori Matsunaga,[‡] Takuya Nakashima,[†] Keisuke Wada,[†] Akira Yamakata,[‡,§] Osamu Ishitani,*[,†] and Kazuhiko Maeda*[,†]

[†]Department of Chemistry, School of Science, Tokyo Institute of Technology, 2-12-1-NE-2 Ookayama, Meguro-ku, Tokyo 152-8550, Japan

[‡]Graduate School of Engineering, Toyota Technological Institute, 2-12-1 Hisakata, Tempaku, Nagoya 468-8511, Japan

[§]PRESTO, Japan Science and Technology Agency, 4-1-8 Honcho, Kawaguchi-shi, Saitama 322-0012, Japan

Supporting Information

ABSTRACT: A metal-free organic semiconductor of mesoporous graphitic carbon nitride (C_3N_4) coupled with a Ru(II) binuclear complex (**RuRu′**) containing photosensitizer and catalytic units selectively reduced CO_2 into HCOOH under visible light ($\lambda > 400$ nm) in the presence of a suitable electron donor with high durability, even in aqueous solution. Modification of C_3N_4 with Ag nanoparticles resulted in a **RuRu′**/Ag/C_3N_4 photocatalyst that exhibited a very high turnover number (>33000 with respect to the amount of **RuRu′**), while maintaining high selectivity for HCOOH production (87−99%). This turnover number was 30 times greater than that reported previously using C_3N_4 modified with a mononuclear Ru(II) complex, and by far the highest among the metal-complex/semiconductor hybrid systems reported to date. The results of photocatalytic reactions, emission decay measurements, and time-resolved infrared spectroscopy indicated that Ag nanoparticles on C_3N_4 collected electrons having lifetimes of several milliseconds from the conduction band of C_3N_4, which were transferred to the excited state of **RuRu′**, thereby promoting photocatalytic CO_2 reduction driven by two-step photoexcitation of C_3N_4 and **RuRu′**. This study also revealed that the **RuRu′**/Ag/C_3N_4 hybrid photocatalyst worked efficiently in water containing a proper electron donor, despite the intrinsic hydrophobic nature of C_3N_4 and low solubility of CO_2 in an aqueous environment.

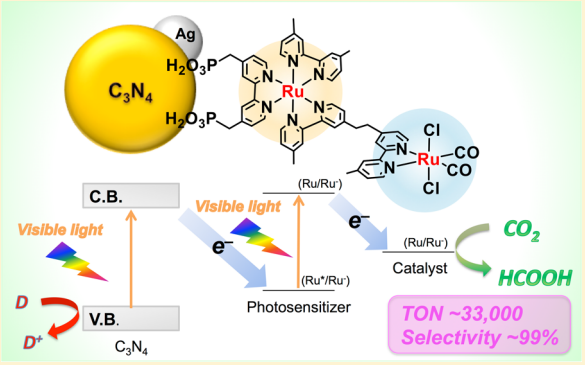

INTRODUCTION

An effective method for converting CO_2—a chemically stable molecule that contributes to the greenhouse effect of the earth's atmosphere—into energy-rich chemicals is of great interest to replace fossil fuels and their concomitant emission of CO_2. Several types of reactions, including catalysis,[1−4] electrochemistry,[5−8] photoelectrochemistry,[9−12] photocatalysis,[13−34] and thermochemical conversion,[35] have been examined. Photocatalytic CO_2 reduction using a semiconductor photocatalyst powder with sunlight, which can occur under mild conditions (e.g., without high temperatures, high pressures, or electricity), may be a feasible method of CO_2 conversion due to its potential simplicity and scalability, as proposed for photocatalytic overall water splitting systems.[36]

Recent advances in heterogeneous photocatalysis using metal oxide semiconductors allowed the reduction of CO_2, even with water as an electron source. However, this photocatalysis requires ultraviolet light due to the large band gaps of the oxides.[20−22] For the efficient utilization of solar energy, a semiconductor that is able to harvest visible light—the main component of the solar spectrum—is required. Frei et al. reported that a polynuclear unit consisting of an oxo-bridged binuclear $ZrOCo^{II}$ group coupled to an iridium oxide nanocluster assembled on an SBA-15 silica mesopore surface could reduce CO_2 into CO and oxidize water into O_2 under visible light.[32] However, the reported turnover number (TON) (46 with respect to $ZrOCo-IrO_x$) was not very large. Applying a visible-light-responsive semiconductor to a photocatalytic CO_2 reduction scheme in combination with a suitable catalytic metal complex seems to be a straightforward platform for carrying out CO_2 reduction,[23−28] but so far none have yielded satisfactory results.

During photosynthesis in green plants, water and CO_2 are converted into oxygen and sugars through two-step photoexcitation of photosystems I and II, which is called the Z-scheme. Mimicking a natural system to achieve "artificial photosynthesis" is challenging, but natural processes can

Received: February 23, 2016
Published: March 30, 2016

DOI: 10.1021/jacs.6b01997
J. Am. Chem. Soc. 2016, 138, 5159−5170

provide useful strategies to develop a photocatalyst for CO_2 reduction. In a Z-scheme system, a wider range of visible light can be used because the energy required to drive each light-absorbing unit can be reduced. Particulate semiconductors have shown a strong ability to oxidize water under visible light,[37−40] but are limited by low selectivity for CO_2 reduction, due to competing proton reduction. In contrast, certain metal complexes, such as Ru(II) binuclear complexes, possess high photocatalytic activity for CO_2 reduction under visible light to produce HCOOH with high turnover numbers (~3000) and high selectivity that are much better than those of semiconductors.[16] However, these metal complexes possess a low oxidation capability (i.e., a strong electron donor is required for obtaining a reasonable reaction rate). The Z-scheme principle could address both of these issues if a binuclear metal complex and a semiconductor are coupled together for use as the reduction and oxidation components, respectively.

This paper describes a nature-inspired artificial Z-scheme CO_2 photoreduction system using an earth-abundant, C/N polymer semiconductor powder, which functions efficiently as the photosystem II (PS(II)) component under visible light irradiation. Recently, a proof-of-concept of the metal-complex/semiconductor Z-scheme for CO_2 reduction was demonstrated to yield HCOOH as the main product with visible light using a Ru(II) binuclear complex (**RuRu′**) and Ag/TaON, but with moderate selectivity (~60%).[33] The present study describes a detailed examination of Z-scheme CO_2 reduction using a metal-free C_3N_4 semiconductor, which was very suitable for a nature-mimicking system because C_3N_4 consists of the earth-abundant elements of carbon and nitrogen. In addition, we examined the impact of metal loading on C_3N_4 to enhance the photocatalytic performance. The hybrid photocatalyst used reduced CO_2 into HCOOH with a catalytic turnover number greater than 33000 and 87−99% selectivity under optimal conditions. These values for turnover number and selectivity are much greater than those reported for similar metal-complex/semiconductor hybrid systems. HCOOH is a useful liquid fuel that can readily be converted into H_2 and CO_2 in the presence of a suitable catalyst.[41] The C_3N_4 may seem unsuitable for use in an aqueous solution because of the intrinsic hydrophobicity of the organic texture.[42] In addition, CO_2 reduction in an aqueous solution is more difficult than in an organic solvent, in terms of both solubility of CO_2 and the high proton concentration that can lead to low selectivity. Interestingly, this new system worked even in water containing a proper electron donor to reduce CO_2 into HCOOH with a TON of ~660 and ~80% selectivity. A schematic illustration of the Z-scheme CO_2 reduction system using C_3N_4 and a binuclear Ru(II) complex is shown in Scheme 1.

Scheme 1. Z-Scheme CO_2 Reduction Using a Hybrid of C_3N_4 and a Binuclear Ru(II) Complex

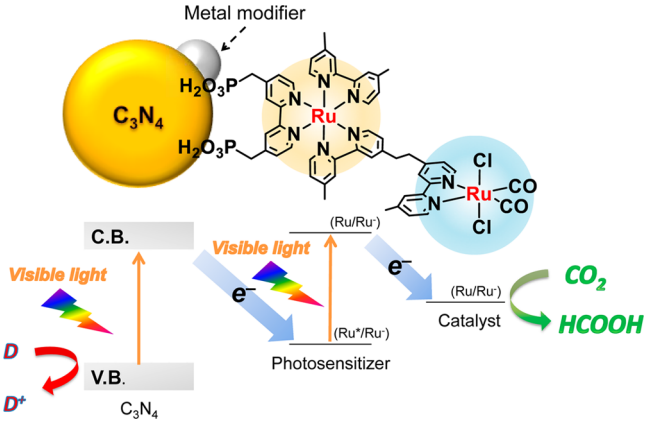

Chart 1. Ru(II) Complexes Used in This Work

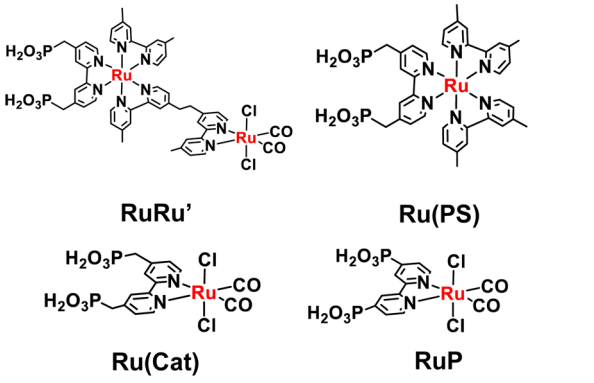

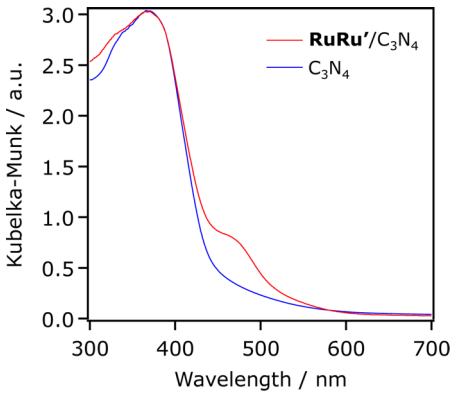

Figure 1. UV−vis diffuse reflectance spectra of **RuRu′** (24.6 μmol g^{-1})/C_3N_4 and unmodified C_3N_4.

RESULTS AND DISCUSSION

Photocatalytic CO_2 Reduction Using RuRu′/C_3N_4 Hybrids. The Ru(II) binuclear complex (**RuRu′**) was immobilized onto the surface of mesoporous graphitic carbon nitride to construct a Z-scheme system. The carbon nitride used had a mesoporous structure (S_{BET} = 180 m^2 g^{-1}, average pore size 12.2 nm, pore volume 0.54 cm^3 g^{-1}), represented as C_3N_4 for simplicity unless otherwise stated. Details of the preparation are described in the Experimental Section. Ruthenium(II) complexes used in this work are shown in Chart 1.

Figure 1 shows UV−vis diffuse reflectance spectra of **RuRu′**/C_3N_4 and unmodified C_3N_4. The C_3N_4 spectrum showed a steep absorption edge near 450 nm, due to band-to-band electron transitions, with a tail extending to 600 nm. Integrating C_3N_4 with **RuRu′** produced a new absorption band centered at 460 nm, due to metal-to-ligand charge transfer (MLCT) excitation of the light-harvesting Ru unit in **RuRu′**. Fourier-transform infrared (FT-IR) spectroscopy revealed two peaks due to the stretching vibrational mode of CO ligands that appeared in the **RuRu′**/C_3N_4 spectrum (1997 and 2062 cm^{-1}, Figure S1). The similar peak positions for **RuRu′**/C_3N_4 and **RuRu′** indicated that the structure of **RuRu′** did not change even after the adsorption on C_3N_4.

Using the **RuRu′**/C_3N_4 hybrid as prepared, photocatalytic CO_2 reduction was performed in an *N*,*N*-dimethylacetamide

DOI: 10.1021/jacs.6b01997
J. Am. Chem. Soc. 2016, 138, 5159−5170

Table 1. Results of Visible Light CO_2 Reduction in a DMA/TEOA Mixed Solution Using C_3N_4 with Various Modifications (λ > 400 nm)[a]

		amount of products/μmol				
entry	photocatalyst	HCOOH	CO	H_2	TON_{HCOOH}	selectivity $_{HCOOH}$
1	C_3N_4	ND	ND	<0.1		
2	**RuRu′**/Al_2O_3	ND	ND	ND		
3	**RuRu′**/C_3N_4	0.6	0.4	0.1	43	52
4[b]	**RuRu′**/C_3N_4	<0.1	ND	0.4		
5[c]	**RuRu′**/C_3N_4	ND	ND	ND		
6	**Ru(PS)**/C_3N_4	ND	<0.1	0.1		
7	**RuP**/C_3N_4	5.8	1.6	0.4	429	74

[a]Reaction conditions: photocatalyst, 4.0 mg (Ru complex loading, 3.4 μmol g^{-1}); solution, 4.0 mL of 4:1 (v/v) DMA/TEOA. Reaction time 5 h. [b]Under an Ar atmosphere. [c]In the dark.

Table 2. Effects of Metal Loading onto C_3N_4 on Visible Light CO_2 Reduction (λ > 400 nm)[a]

		amount of products/μmol				
entry	photocatalyst	HCOOH	CO	H_2	TON_{HCOOH}	$selectivity_{HCOOH}$
1	**RuP**/C_3N_4	5.8	1.6	0.4	429	74
2	**RuP**/Ag/C_3N_4	19.2	0.2	0.3	1428	98
3	**RuRu′**/C_3N_4	0.6	0.4	0.1	43	52
4	**RuRu′**/Ag/C_3N_4	42.3	<0.1	0.3	3110	>99
5[b]	**RuRu′**/Ag/C_3N_4	ND	ND	ND		
6[c]	**RuRu′**/Ag/C_3N_4	<0.1	ND	6.4		
7	Ag/C_3N_4	1.2	ND	2.2		36
8	**RuRu′**/Cu/C_3N_4	0.3	ND	0.2	22	60
9	**RuRu′**/Au/C_3N_4	1.7	<0.1	17.3	125	9
10	**RuRu′**/Pt/C_3N_4	ND	ND	17.5		
11	Cu/C_3N_4	ND	ND	0.1		
12	Au/C_3N_4	0.5	ND	13.2		4
13	Pt/C_3N_4	ND	ND	26.7		

[a]Reaction conditions: photocatalyst, 4.0 mg (Ru complex loading, 3.4 μmol g^{-1}; metal loading, 5.0 wt %); solution, 4.0 mL of 4:1 (v/v) DMA/TEOA. Reaction time 5 h. [b]Dark conditions. [c]Under an Ar atmosphere.

(DMA)/triethanolamine (TEOA) mixed solution under visible light (λ > 400 nm). DMA was used as the solvent because it had been shown to maximize the catalytic performance of C_3N_4 modified with a mononuclear Ru(II) complex for CO_2 reduction.[26] DMA is known to be a good solvent for CO_2 reduction in homogeneous systems.[18] Table 1 summarizes the results of CO_2 reduction reactions. The C_3N_4 alone showed no activity under the present reaction conditions (entry 1). Combining **RuRu′** with Al_2O_3, which is an insulator, also did not result in any product (entry 2). However, combining **RuRu′** with C_3N_4 resulted in observable HCOOH and CO formation with TONs of 43 and 32, respectively, and selectivities of 52% and 38%, respectively, after 5 h of visible light irradiation (entry 3). Control experiments showed that HCOOH formation on **RuRu′**/C_3N_4 was negligible when either CO_2 or visible light was absent (entries 4 and 5). Modification with only a Ru mononuclear complex as a model of the photosensitizer unit, **Ru(PS)**, did not produce a detectable amount of HCOOH (entry 6). The C_3N_4 modified with a catalytically active, mononuclear Ru(II) complex, such as the optimal mononuclear Ru(II) complex Ru{4,4′-$(PO_3H_2)_2$-2,2′-bibyridine}$(CO)_2Cl_2$ (**RuP**)[26] (see Chart 1), produced HCOOH and CO photocatalytically (entry 7). The amount of products was higher than that using **RuRu′**/C_3N_4 (entry 3), suggesting the photocatalytic CO_2 reduction using the Z-scheme system was not very efficient at this time, compared to C_3N_4 modified with a mononuclear Ru(II) complex.

Effect of Metal Loading on C_3N_4 upon Photocatalytic CO_2 Reduction. Although **RuRu′**/C_3N_4 and **RuP**/C_3N_4 photocatalyzed CO_2 reduction upon exposure to visible light, the product selectivity was not high (Table 1, entries 3 and 7). Metal loading on a semiconductor improves the rate of some photocatalytic reactions, which can lead to high selectivity.[20,22] To investigate the impact of metal loading on photocatalytic performance, C_3N_4 was modified by silver to serve as an electron sink, but not function efficiently as a cocatalyst for H_2 evolution due to the relatively large overpotential.[20] Ag also is known to function as an electrocatalyst for CO_2 reduction.[6] Therefore, Ag was first tested and loaded onto C_3N_4 using a conventional impregnation method (followed by H_2 reduction at 473 K). After Ag loading, **RuRu′** and **RuP** were adsorbed in the same manner.

Table 2 lists the photocatalytic activities of C_3N_4 modified with various metals and **RuRu′** (or **RuP**). Ag modification was found to improve the activity of **RuP**/C_3N_4 by 3.3-fold (entries 1 and 2), with very high selectivity for HCOOH (98%). However, this was not as high as that observed in **RuRu′**/C_3N_4, where the activity was enhanced upon Ag loading by approximately 70-fold (entries 3 and 4), suggesting Ag has an extremely positive impact on the Z-scheme-type system. Highly selective HCOOH generation over **RuRu′**/Ag/C_3N_4 was also observed even under >480 nm irradiation, although the amount of produced HCOOH was much lower than that under >400 nm irradiation (Table S1). When using **RuRu′**/Ag/C_3N_4, the produced amounts of HCOOH were 2.2 times higher than

DOI: 10.1021/jacs.6b01997
J. Am. Chem. Soc. 2016, 138, 5159−5170

those obtained using **RuP**/Ag/C_3N_4, clearly demonstrating the feasibility of the Z-scheme-type system.

Next, we conducted some control experiments using **RuRu′**/Ag/C_3N_4. First of all, no reaction occurred under dark conditions (entry 5). Under an Ar atmosphere, HCOOH generation was negligible, but H_2 evolution was evident (entry 6). In the absence of **RuRu′**, Ag/C_3N_4 produced HCOOH and H_2 under the present reaction conditions (entry 7), indicating that Ag also can function to generate HCOOH and H_2. In this situation, isotope tracer experiments with $^{13}CO_2$ confirmed that the origin of the HCOOH produced was CO_2 (Figure S2), although selectivity toward HCOOH was only 36% due to significant H_2 evolution.

Interestingly, loading other metals that belong to the same XI elemental group as Ag (i.e., Cu and Au) onto C_3N_4 did not yield any appreciable conversion (entries 8 and 9), although **RuRu′**/Au/C_3N_4 generated H_2 dominantly, accompanied by HCOOH production that was ∼3 times greater than that of the nonmetalized sample. This result strongly suggests that photogenerated electrons in the conduction band of C_3N_4 were consumed by proton reduction with the aid of Au. Modification of C_3N_4 with Pt, which is a well-known cocatalyst for proton reduction, also resulted in efficient H_2 evolution, even under a CO_2 atmosphere, and no CO_2 reduction activity (entry 10). Without **RuRu′**, these metal-loaded C_3N_4 samples produced H_2 predominantly even under a CO_2 atmosphere, except that loaded with Cu, which generated a low level of H_2 (entry 11). The rates of H_2 evolution were much faster than that observed for the Ag-loaded sample (entries 7, 12, and 13). Among them, Au/C_3N_4 without **RuRu′** produced a detectable amount of HCOOH under the present reaction conditions (entry 12), although it did not work as efficiently as Ag/C_3N_4 did (entry 7).

Ruthenium(II) trisdiimine complexes, such as **Ru(PS)**, produce emissions centered at around 640 nm from the lowest ^{3}MLCT excited state.[43,44] To accomplish Z-scheme CO_2 reduction using C_3N_4 and **RuRu′**, electron transfer from the conduction band of C_3N_4 to the sensitizing Ru unit in **RuRu′** (i.e., reductive quenching) is essential. In our previous study on Z-scheme CO_2 reduction using Ag/$CaTaO_2N$ modified with **RuRu′**, emission decay measurements using the model complex of **Ru(PS)** indicated that Ag nanoparticles exhibiting optimal distribution are essential to facilitate interfacial electron transfer from the conduction band of $CaTaO_2N$ to **RuRu′**.[34] We tried to examine the effect of metals loaded on C_3N_4 on the photochemical process through emission decay measurements. Due to the significant contribution of light scattering by the C_3N_4 suspension, unfortunately, we could not analyze the emission decay curves obtained.[45] Nevertheless, our previous result[34] suggests that reductive quenching of the excited state of the photosensitizer unit occurs, once the loaded Ag accepts electrons from the conduction band of a semiconductor. Electron transfer from C_3N_4 to the loaded Ag (as well as to other metals) is strongly supported by the results of photocatalytic reactions (Table 2). In the case of the best performing Ag promoter, the evidence of electron transfer from C_3N_4 to the loaded Ag will be discussed on the basis of the results of time-resolved infrared absorption spectroscopy.

In addition to the forward electron transfer, investigating possible back electron transfer path(s) is important. First, it should be noted that electron injection from the excited state of **Ru(PS)** (E_{ox}* = −1.30 V)[33] to the conduction band of C_3N_4 (E_{CB} = −1.65 V vs Ag/$AgNO_3$ at pH 7)[24] was thermodynamically unfavorable. Furthermore, ultrafast electron injection from ^{1}MLCT of **Ru(PS)** to the conduction band of a semiconductor can be suppressed effectively using a methylene spacer between the semiconductor and **Ru(PS)**.[46,47] These results suggest that electron transfer from the excited state of **Ru(PS)** to the conduction band of C_3N_4 (i.e., the oxidative quenching path) was largely suppressed in this system. We also studied possible electron and/or energy transfer from the excited state of **Ru(PS)** to metals. As shown in Figure 2, no noticeable change

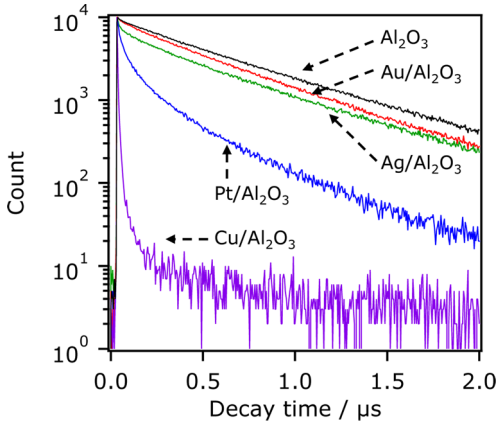

Figure 2. Results of emission decay measurements of **Ru(PS)** on Al_2O_3 with various metals in DMA. Before the experiment, reductive quenching of the excited state of **Ru(PS)** by TEOA was determined to be negligible. The emission was monitored at 700 nm with excitation light at λ_{ex} = 444 nm.

in emission decay occurred when using **Ru(PS)** on Al_2O_3 with or without Ag and Au loading. In contrast, for Pt and Cu loading, emission decay from the excited state of **Ru(PS)** adsorbed on Al_2O_3 was more pronounced, as compared to that from the excited state of **Ru(PS)** modified with Au and Ag (as well as that from the excited state of the unmodified sample). These results indicate that electron and/or energy transfer from the excited state of **Ru(PS)** to the Ag (or Au) loaded did not occur, but was efficient when Pt or Cu was applied.

On the basis of the results of photocatalytic reactions and emission decay measurements, it is concluded that a metal modifier for the Z-scheme system has to possess a large overpotential for proton reduction to suppress H_2 evolution, and to be resistant to electron and/or energy acceptance from the excited-state photosensitizer unit of **RuRu′**. Because Ag satisfied both of the requirements, it was best among the four metals tested at promoting Z-scheme photocatalytic CO_2 reduction.

Thomas et al. have reported that the surface of C_3N_4 is terminated with amino groups, which are potential sites for anchoring functional units.[48] As discussed in our previous papers,[25,27] we think that hydrogen bonds are formed between $-NH_2$ groups on C_3N_4 and $-PO_3H_2$ groups derived from Ru(II) complexes. Therefore, one may expect a similar situation when **Ru(PS)**, which has $-CH_2PO_3H_2$ groups, is used. However, we could not elucidate the exact location of **Ru(PS)** (or **RuRu′**) on Ag/C_3N_4. Considering the fact that the Z-scheme CO_2 reduction was promoted by Ag loading on C_3N_4, it is likely that the relative location of **RuRu′** and Ag nanoparticles is close enough to afford electron transfer between the two.

DOI: 10.1021/jacs.6b01997
J. Am. Chem. Soc. 2016, 138, 5159−5170

Effect of Ag Loading on C_3N_4 on Photocatalytic CO_2 Reduction. When C_3N_4 was modified with Ag prior to immobilization of **RuRu′**, performance was improved significantly. Therefore, the promotional effect of Ag was investigated in more detail. As shown in Figure 3, the rate of HCOOH production increased sharply with the loading amount of Ag and reached a plateau at 1.5−5.0 wt %, beyond which it began to drop.

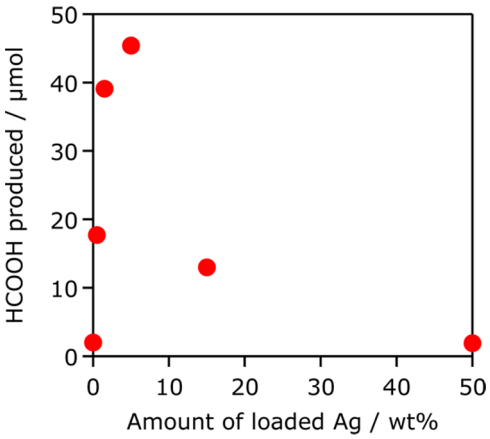

Figure 3. Photocatalytic performance for CO_2 reduction that generated HCOOH over **RuRu′** (4.7 μmol g^{-1})/Ag/C_3N_4 as a function of the loading amount of Ag. Reaction conditions: 4.0 mg of photocatalyst, 4.0 mL of 4:1 (v/v) DMA/TEOA. Reaction time 5 h.

To investigate the relationship between activity and photocatalyst structure, the hybrids were subjected to physicochemical analyses using X-ray diffraction (XRD), diffuse reflectance spectroscopy (DRS), X-ray photoelectron spectroscopy (XPS), transmission electron microscopy (TEM), and nitrogen adsorption/desorption measurements. Figure 4 shows XRD patterns and DRS spectra of Ag/C_3N_4 with different Ag loadings. At loadings up to 5.0 wt %, no change was seen in XRD patterns or DRS spectra. However, a further increase in loading amount generated clear diffraction peaks assigned to metallic Ag, accompanied by a new absorption band at 500−800 nm, due to the localized surface plasmonic resonance of Ag and/or the metallic nature of Ag. The XPS analysis indicated that the valence state of Ag in the 5.0 wt % Ag-loaded C_3N_4 was entirely zerovalent (Figure S3). Thus, the physicochemical state of Ag loaded on C_3N_4 appears to be metallic. However, even at a relatively high loading amount (5.0 wt %), which induced the greatest photocatalytic performance, no sign of metallic Ag formation was seen in the XRD and DRS results. Thus, we performed TEM observations of the 5.0 wt % Ag-loaded C_3N_4, which indicated that Ag nanoparticles with an average size of 6.9 nm were distributed on the surface of C_3N_4, as shown in Figure 5. Below 5.0 wt % Ag loading, it is therefore reasonable to expect that smaller Ag nanoparticles, which do not exhibit any plasmonic absorption in the visible light region, are loaded on the surface of C_3N_4.

Loading Ag onto C_3N_4 somewhat altered the original porous structure of C_3N_4, reducing the specific surface area, pore size, and pore volume, as shown in Figure 6 and Table 3. This indicates that mesopores existing in C_3N_4 were filled with Ag deposits, but the effect was not very sensitive to the Ag loading amount. Presumably, at greater Ag loadings, Ag was deposited not only inside the pores but also on the external surface of C_3N_4, resulting in aggregation as evidenced by XRD and UV−vis analyses (Figure 4). This was the main reason for the decrease in activity observed at greater Ag loadings (Figure 3), because the aggregated Ag at higher loading can hinder light absorption by C_3N_4 due to a filtering effect.

The role of Ag with C_3N_4 was also studied using time-resolved infrared absorption (TR-IR) spectroscopy, which can assess photogenerated charge carriers in a semiconductor material.[40,49−54] Figure 7 shows transient absorption spectra for C_3N_4, which were irradiated with pulses at 355 nm under vacuum. Upon band gap photoexcitation of C_3N_4, a broad absorption was observed over the entire wavenumber region from 20000 to 1000 cm^{-1}. Absorption bands appearing in the visible to near-IR region (20000−3000 cm^{-1}) were assigned to deeply trapped electrons and/or holes.[53,54] In contrast, the absorptions in the mid-IR region (3000−1000 cm^{-1}) were assigned to free or shallowly trapped electrons.[49] Essentially the same result was obtained for Ag/C_3N_4.

The decay kinetics of photogenerated free or shallowly trapped electrons in C_3N_4 and Ag/C_3N_4 were also examined by recording the change in transient absorption intensity at 2000 cm^{-1}. Surprisingly, long-lived charge carriers with lifetimes longer than milliseconds were observed (Figure 8), which could account for the high potential of C_3N_4 as a semiconductor photocatalyst. However, the decay at 2000 cm^{-1} was more pronounced in Ag/C_3N_4 than in C_3N_4. More importantly, the accelerated decay by Ag loading tended to be less pronounced at higher wavenumbers. This strongly suggests that shallowly trapped electrons in C_3N_4 are able to move to the loaded Ag, while deeply trapped ones are not. The results of emission

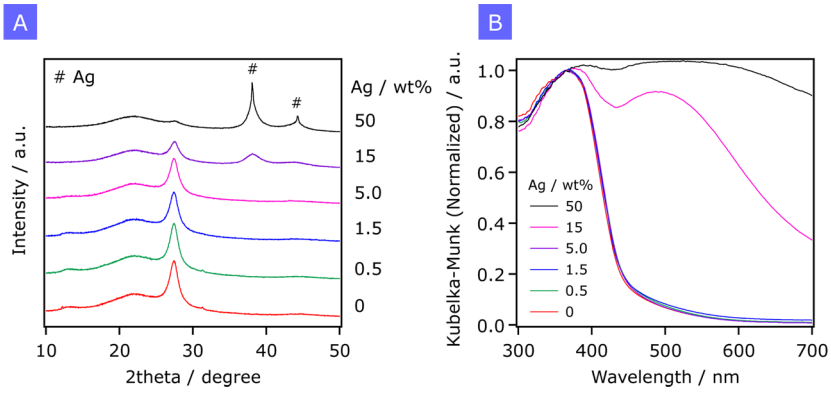

Figure 4. (A) XRD patterns and (B) UV−vis diffuse reflectance spectra of C_3N_4 modified with different amounts of Ag.

DOI: 10.1021/jacs.6b01997
J. Am. Chem. Soc. 2016, 138, 5159−5170

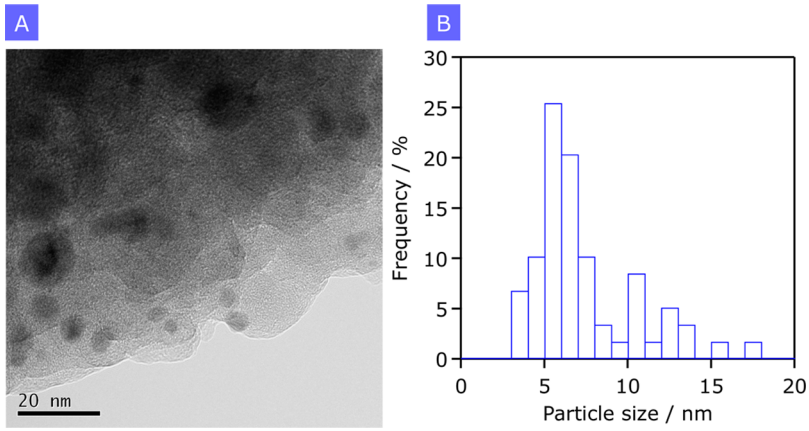

Figure 5. (A) TEM image of Ag (5.0 wt %)/C_3N_4 and (B) the corresponding size distribution of Ag on C_3N_4.

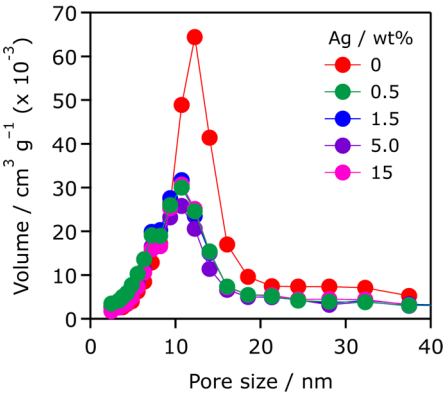

Figure 6. Barrett–Joyner–Halenda (BJH) pore size distributions of C_3N_4 modified with different amounts of Ag.

Table 3. Effects of Ag Loading onto C_3N_4 on Pore Wall Structures

entry	Ag loading amount/wt %	specific surface area/m^2 g^{-1}	pore diameter/nm	pore volume/cm^3 g^{-1}
1	0	180	12.2	0.54
2	0.5	124	10.7	0.35
3	1.5	122	10.7	0.35
4	5.0	103	10.7	0.29
5	15	109	10.7	0.32

decay measurements, time-resolved infrared spectroscopy, and photocatalytic CO_2 reduction indicated that Ag acted as an electron pool and a mediator of electron transfer from C_3N_4 to **Ru(PS)**, thereby enhancing the photocatalytic ability of CO_2 reduction in this Z-scheme system.

Optimization of RuRu′/Ag/C_3N_4 Hybrids for Photocatalytic CO_2 Reduction and Comparison with Other Systems. The amount of adsorbed **RuRu′** exerted a strong influence on photocatalytic performance. As shown in Figure 9A, the HCOOH production rate increased with the loading amount of **RuRu′** up to 1.5 μmol g^{-1} and then underwent saturation. However, TON_{HCOOH} decreased monotonically with increasing **RuRu′**. At a loading of 0.5 μmol g^{-1}, TON_{HCOOH} reached 33000 after 48 h (Figure 9B), which is a 30-fold greater value than those achieved by previous studies using C_3N_4 modified with a mononuclear Ru(II) complex under identical reaction conditions.[26] Even with the use of an organic semiconductor consisting of carbon and nitrogen, the origin of HCOOH generated was confirmed to come from CO_2 through an isotope tracer experiment using $^{13}CO_2$ (Figure 10).

Figure S4 shows UV–vis diffuse reflectance spectra of **RuRu′**/Ag/C_3N_4 hybrids with different **RuRu′** loadings. The MLCT absorption due to the sensitizing unit of **RuRu′** became more pronounced as the loading amount of **RuRu′** increased. Therefore, the increase in HCOOH production from 0.5 to 1.5 μmol g^{-1} was attributed to improved light-harvesting by the sensitizing unit of **RuRu′**. However, a further increase in the

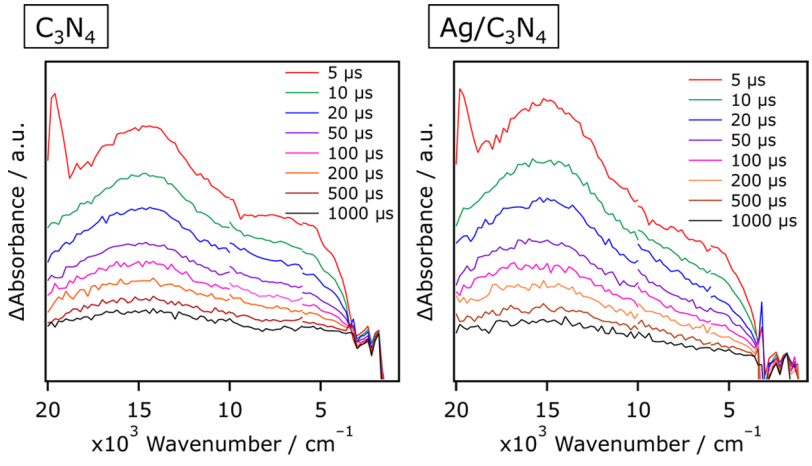

Figure 7. Transient absorption spectra for C_3N_4 and Ag/C_3N_4 recorded by 355 nm laser pulse excitation under vacuum.

DOI: 10.1021/jacs.6b01997
J. Am. Chem. Soc. 2016, 138, 5159–5170

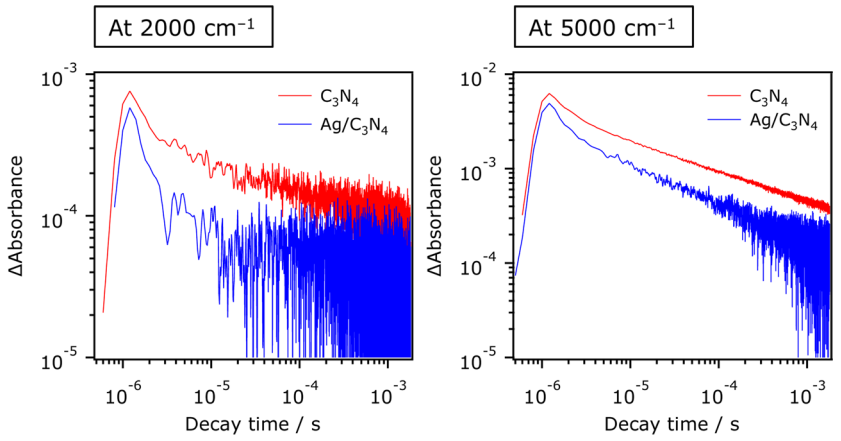

Figure 8. Decay curves of transient absorption intensity at different wavenumbers for C_3N_4 and Ag/C_3N_4.

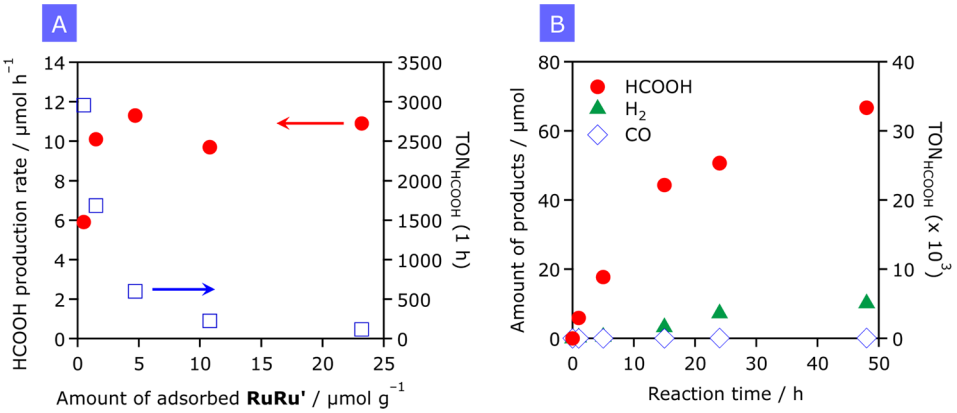

Figure 9. (A) Photocatalytic performance of CO_2 reduction that generated HCOOH over **RuRu′**/Ag (5.0 wt %)/C_3N_4 as a function of the loading amount of **RuRu′**. (B) Time course of CO_2 reduction over **RuRu′** (0.5 μmol g^{-1})/Ag (5.0 wt %)/C_3N_4. Reaction conditions: 4.0 mg of photocatalyst, 4.0 mL of 4:1 (v/v) DMA/TEOA.

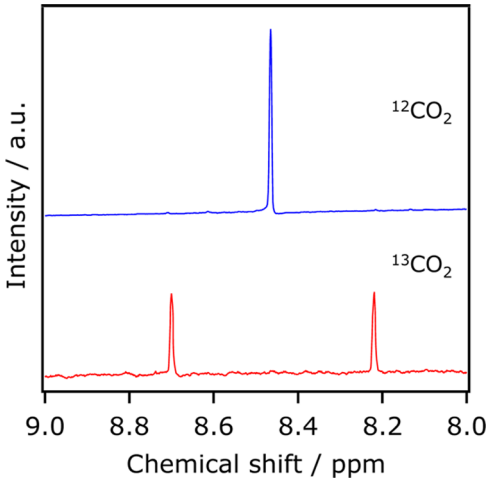

Figure 10. No-D NMR spectra of a reacted solution [2.0 mL of 4:1 (v/v) DMA/TEOA] containing 4.0 mg of **RuRu′** (3.4 μmol g^{-1})/Ag (5.0 wt %)/C_3N_4, obtained after filtration. The photocatalyst suspension was subjected to visible light irradiation from a 400 W high-pressure mercury lamp with a $NaNO_2$ solution filter for 12 h under $^{13}CO_2$ (660 Torr) and saturated unlabeled CO_2. The doublet observed was attributed to protons bound to the ^{13}C atom in $H^{13}COOH$.

loading amount of **RuRu′** (>1.5 μmol g^{-1}) did not enhance HCOOH production. In this situation, unlike that in the lower adsorption region, the density of the excited state of **Ru(PS)** should be sufficiently high, limiting electron transfer from C_3N_4 to the excited state of **Ru(PS)**.

The AQY of the present hybrid system measured using monochromatic light from a 300 W xenon lamp was 5.2% at 400 nm, which is slightly lower than that recorded previously using a mononuclear Ru(II) complex (5.7% at 400 nm).[26] However, the use of a 400 W Hg lamp with a $NaNO_2$ solution filter resulted in an initial rate of HCOOH generation by the optimized **RuRu′**/Ag/C_3N_4 (11.3 μmol h^{-1}) that was 1.3 times faster than that using the optimized Ru(II) mononuclear complex/C_3N_4 hybrid (8.8 μmol h^{-1}), reported previously to produce 5.7% at 400 nm.[26] Assuming that photons with wavelengths longer than 400 nm are absorbed by the reactant suspension, the present Z-scheme system (two-photon system) would be at least 2.6 times (2 × 1.3) more efficient than the previous system (one-photon system). Since the Hg lamp used in the present study is more intense compared to the Xe lamp used for AQY measurements, photocatalytic activity would be strongly influenced by the light intensity. More concretely, under low light intensity conditions, the activity of the Z-scheme system may be lower than that of the ruthenium(II) mononuclear complex/C_3N_4 hybrid systems.

Another important observation of the present hybrid system was the degradation of HCOOH production with time; production leveled off after 15 h, accompanied by H_2 evolution (Figure 9B). Since C_3N_4 is a very stable photocatalyst for H_2

DOI: 10.1021/jacs.6b01997
J. Am. Chem. Soc. 2016, 138, 5159−5170

Table 4. Comparison of Photocatalytic Activity for Visible Light CO_2 Reduction Using Carbon Nitrides and Ru Complexes (λ > 400 nm)[a]

entry	Ru complex	loading amount/μmol g^{-1}	type of C_3N_4	specific surface area/m^2 g^{-1}	amount of HCOOH/μmol	TON_{HCOOH}
1[b]	**Ru(Cat)**	3.9	7 nm pores	241	ND	
2[b]	**Ru(Cat)**	2.3	bulk	6	ND	
3[b]	**Ru(Cat)**	3.9	12 nm pores	180	1.6	50
4[c]	**RuP**	3.5	7 nm pores	241	2.8	201
5[c]	**RuP**	2.9	bulk	6	0.4	39
6[c]	**RuP**	3.4	12 nm pores	180	5.8	429
7[c,d]	**RuRu′**	3.4	7 nm pores	241	35.3	2592
8[c,d]	**RuRu′**	3.4	bulk	6	2.7	196
9[c,d]	**RuRu′**	3.4	12 nm pores	180	42.3	3110

[a]Reaction conditions: photocatalyst, 4.0−8.0 mg; 4.0 mL of solution. Reaction time 5 h. [b]Reaction conditions: photocatalyst, 8.0 mg; solution, 4:1 (v/v) MeCN/TEOA. [c]Reaction conditions: photocatalyst, 4.0 mg; solution, 4:1 (v/v) DMA/TEOA. [d]A 5.0 wt % concentration of Ag was loaded on C_3N_4 before **RuRu′** was adsorbed.

evolution in the presence of TEOA as an electron donor,[55] this deactivation is likely to originate from the reduction part. We first examined the possibility of deactivation of the Ag and C_3N_4 components in this photocatalyst after 48 h of reaction (see Figure 9B) by means of XRD, FT-IR, DRS, and XPS measurements. As shown in Figure S5, no significant difference could be identified in XRD patterns, FT-IR spectra, and DRS spectra. These results indicate that the crystal structure, heptazine-based C/N framework, and resulting optical property of the C_3N_4 component remained unchanged. The result of XPS measurements showed that the peak position of the Ag 3d photoelectron signal did not undergo a shift (Figure S6). This means that the valence state of Ag nanoparticles on C_3N_4 was kept even after 48 h of photocatalytic reaction. As discussed earlier, Ag on C_3N_4 promoted interfacial electron transfer from C_3N_4 to the excited state of **RuRu′**. However, it also acts as a cocatalyst for H_2 formation (Table 2, entry 7). In addition, reaction using a **RuRu′**/Ag/C_3N_4 hybrid under an Ar atmosphere, where **RuRu′** does not function as a CO_2 reduction photocatalyst, gave H_2 as the major product (Table 2, entry 6). Thus, when **RuRu′** loses functionality as a CO_2 reduction (photo)catalyst due to decomposition and/or structural change, the functionality of Ag could switch from an interfacial electron transfer promoter to a H_2 evolution site. If this idea is correct, the selectivity for HCOOH generation should be improved by an increase in the loading amount of **RuRu′**. In fact, we confirmed that Ag/C_3N_4 modified with 1.5 μmol g^{-1} **RuRu′** exhibited very high selectivity for HCOOH even after 48 h of visible light irradiation, in contrast to an analogue modified with 0.5 μmol g^{-1} **RuRu′** (Figure S7). Although analyzing the structure of **RuRu′** was difficult after the long-time run due primarily to the low concentration, the failure of the **RuRu′** functioning appeared to contribute to the deactivation of photocatalytic CO_2 reduction by the **RuRu′**/Ag/C_3N_4 hybrid photocatalyst.

We also investigated the possible impact of **RuRu′** desorption on the photocatalyst deactivation, and measured the amounts of **RuRu′** desorbed during the reaction. Using **RuRu′** (3.4 μmol g^{-1})/Ag (5.0 wt %)/C_3N_4, approximately 30% of the initially adsorbed complexes underwent desorption just after CO_2 bubbling in a DMA/TEOA mixed solution. However, the desorption amount remained almost unchanged even after 24 h of visible light irradiation. Considering the fact that this photocatalyst stably generated HCOOH at least for 5 h, it appears that the desorption of **RuRu′** did not directly contribute to the activity drop of this hybrid system.

The photocatalytic performance for CO_2-to-HCOOH conversion was compared among types of carbon nitride with different textural properties because the structure of a semiconductor photocatalyst is known to affect activity.[36] Optimization studies of the pore-wall structure of mesoporous graphitic carbon nitride with **Ru(Cat)** for visible light CO_2 reduction in a solution of acetonitrile and TEOA showed that the activity increased with the specific surface area by introducing mesopores into graphitic carbon nitride. However, the introduction of an excess amount of mesoporosity resulted in shrinkage of the carbon nitride walls, increasing the density of defects and thereby lowering the activity.[25] As listed in Table 4, nonporous bulk carbon nitride and a mesoporous analogue with a high specific surface area showed negligible activity (entries 1 and 2), compared to the optimized mesoporous carbon nitride (entry 3). Even with the use of the optimal mononuclear Ru(II) complex **RuP** and DMA as the solvent,[26] these "inferior" carbon nitrides (entries 4 and 5) did not outperform the optimized one (entry 6). In contrast to systems with similar mononuclear Ru(II) complexes, a relatively high level of HCOOH generation was observed when they were modified with Ag and **RuRu′** to form a Z-scheme CO_2 reduction system (entries 7 and 8), although the activities were not as high as that of the optimized carbon nitride (entry 9). These results suggest that this Z-scheme system could be used for semiconductors that have suboptimal properties because application of the Z-scheme principle can realize the full potential of a semiconductor.

CO_2 Reduction over RuRu′/Ag/C_3N_4 Hybrids in Aqueous Solution. For practical applications, a photocatalytic CO_2 reduction system, which can operate in water, is needed. The optimized C_3N_4-based hybrid material functioned as a photocatalyst for CO_2 reduction under visible light, even in water containing a suitable electron donor. Figure 11 shows a typical time course for CO_2 reduction in aqueous solution containing 10 mM ethylenediaminetetraacetic acid disodium salt dihydrate (EDTA·2Na) as an electron donor, which was applied to H_2 evolution using carbon nitride.[55] The main product was HCOOH, accompanied by H_2 as a byproduct. Carbon monoxide formation was negligible, even after an extended period of irradiation. The HCOOH production gradually degraded with time, along with the release of H_2.

It should also be noted that, as displayed in Table 5, C_3N_4 modified with **RuP** did not work efficiently under the present conditions, regardless of Ag loading (entries 2 and 3) compared to the Z-scheme system (entry 1), even though it worked

DOI: 10.1021/jacs.6b01997
J. Am. Chem. Soc. 2016, 138, 5159−5170

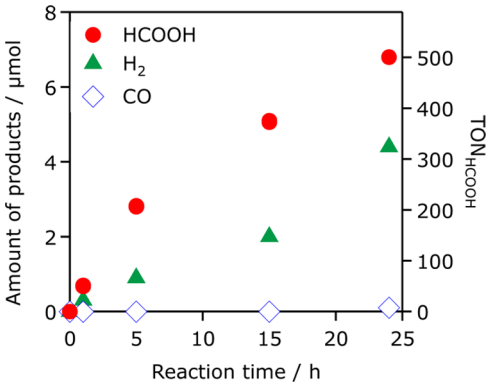

Figure 11. Time course of CO_2 reduction over **RuRu′** (3.4 μmol g^{-1})/Ag (1.5 wt %)/C_3N_4. Reaction conditions: 4.0 mg of photocatalyst, 4.0 mL of aqueous EDTA·2Na solution (10 mM).

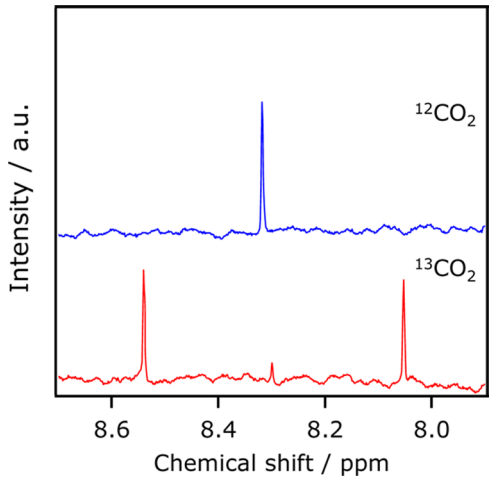

Figure 12. No-D NMR spectra of a reactant solution (2.0 mL of 10 mM aqueous EDTA·2Na) containing 4.0 mg of **RuRu′** (3.4 μmol g^{-1})/Ag (1.5 wt %)/C_3N_4, measured after filtration. The photocatalyst suspension was subjected to visible light irradiation from a 400 W high-pressure mercury lamp with a $NaNO_2$ solution filter for 15 h under $^{13}CO_2$ (680 Torr) and saturated unlabeled CO_2.

efficiently in a mixed solution of DMA and TEOA (Table 2). This result clearly indicates that the Z-scheme principle is essential to achieving visible light CO_2 reduction using a hybrid of a Ru(II) complex and carbon nitride.

Isotope-labeling experiments with $^{13}CO_2$ were used to investigate the origin of the HCOOH produced during the reaction. Photocatalytic reactions were conducted in the same manner but under 680 Torr of $^{13}CO_2$. After 15 h of visible light irradiation, the reactant suspension was filtered to remove the solid photocatalyst, and the resultant supernatant solution was analyzed using NMR spectroscopy. Figure 12 shows no-deuterium proton (No-D) NMR spectra of reactant solutions after the reaction. When $^{12}CO_2$ was used as the reactant gas, only a singlet was observed. In contrast, a doublet (J^{13}_{CH} = 188 Hz), assigned to protons bound to ^{13}C in $H^{13}COOH$, was observed between 8.54 and 8.05 ppm. The ratio of $H^{13}COOH$ to $H^{12}COOH$ was approximately 20, demonstrating that $H^{13}COOH$ was the major product. In this case, 96% of HCOOH generated came from CO_2.

Thus, **RuRu′**/Ag/C_3N_4 is capable of reducing CO_2 to HCOOH under visible light, even in aqueous solution. The results also showed that other electron donors, such as potassium oxalate[56] and sodium ascorbate, were useful in CO_2-to-HCOOH conversion using **RuRu′**/Ag/C_3N_4 (Table 6). Among the electron donors tested, potassium oxalate had the best performance in terms of TON (662) and selectivity for HCOOH generation (75%) after 24 h of visible light irradiation (Figure S8).

Recently, Xu et al. reported that graphitic carbon nitride modified with layered double hydroxide nanosheets and palladium nanoparticles converted CO_2 into CH_4 in aqueous solution under visible light, with a TON of 3.8 (with respect to the loaded Pd).[29] According to that study, selectivity toward CH_4 was only ∼18%, due to significant H_2 evolution (∼81% selectivity). The new system developed in the present study using **RuRu′**/Ag/C_3N_4 produced superior TON values (660 for 24 h) and selectivity (∼80%) compared to those from the previous photocatalyst. However, this new system still relies on a sacrificial electron donor for CO_2 reduction (Table 6), and did not work at all in pure water, due primarily to slow water oxidation kinetics.[57,58] Construction of a suitable reaction site for water oxidation seems to be the key for C_3N_4 to achieve artificial photosynthetic CO_2 reduction. In fact, Wang et al. very recently achieved overall water splitting without any sacrificial reagent using graphitic carbon nitride coloaded with Pt and PtO_x, which served respectively as water reduction and oxidation cocatalysts.[59] It is also expected that recent progress on morphological and electronic engineering of carbon nitride[60−62] will put forward further improvement of the photocatalytic performance of the material for CO_2 reduction, as the lifetime of electron/hole pairs in C_3N_4 depends strongly on the physicochemical properties. These possibilities are now under investigation.

■ CONCLUSIONS

An artificial Z-scheme system inspired by natural photosynthesis in green plants was developed using a metal-free semiconductor that exhibited high selectivity toward HCOOH production via CO_2 reduction under visible light. The results showed that Ag-loaded mesoporous C_3N_4 coupled with a Ru(II) binuclear complex exhibited high selectivity for CO_2-to-HCOOH conversion (87−99%), which functioned

Table 5. Results of Visible Light CO_2 Reduction in Aqueous EDTA Using C_3N_4 with Various Modifications (λ > 400 nm)[a]

		amount of products/μmol				
entry	photocatalyst	HCOOH	CO	H_2	TON_{HCOOH}	$selectivity_{HCOOH}$
1	**RuRu′**/Ag/C_3N_4	2.7	0.1	0.9	200	75
2	**RuP**/C_3N_4	ND	ND	<0.1		
3	**RuP**/Ag/C_3N_4	0.2	ND	0.5	12	24

[a]Reaction conditions: photocatalyst, 4.0 mg (Ru complex loading, 3.4 μmol g^{-1}; Ag loading, 1.5 wt %); solution, 4.0 mL of 10 mM aqueous EDTA·2Na. Reaction time 5 h.

DOI: 10.1021/jacs.6b01997
J. Am. Chem. Soc. 2016, 138, 5159−5170

Table 6. Results of Visible Light CO_2 Reduction in Aqueous Solution Using RuRu′/Ag/C_3N_4 with Various Electron Donors (λ > 400 nm)[a]

		amount of products/μmol				
entry	electron donor	HCOOH	CO	H_2	TON_{HCOOH}	$selectivity_{HCOOH}$
1	EDTA·2Na	5.1	<0.1	2.2	371	70
2	sodium ascorbate	1.8	ND	0.3	131	86
3	potassium oxalate	8.0	ND	1.7	586	83
4	water	ND	ND	ND		

[a]Reaction conditions: photocatalyst, **RuRu′** (3.4 μmol g^{-1})/Ag (1.5 wt %)/C_3N_4 4.0 mg; 4.0 mL of an aqueous solution containing the electron donor (10 mM). Reaction time 15 h.

according to the Z-scheme principle. This hybrid produced a TON of ~33000 for 48 h, indicating that it was much more efficient than analogues modified with a mononuclear Ru(II) complex. This hybrid system worked even in aqueous solution with high durability, presenting the first example of applying a metal-free organic semiconductor to a Z-scheme CO_2 reduction system functional in water. The results of photocatalytic reactions, emission decay measurements, and time-resolved infrared absorption spectroscopy indicated that the key to high efficiency in this Z-scheme system was the use of a modifier that had a large overpotential for H_2 evolution and mediated interfacial electron transfer from a semiconductor to the excited state of the light-harvesting metal complex, while suppressing back electron and/or energy transfer.

EXPERIMENTAL SECTION

Purification of Solvents. DMA was dried over 4 Å molecular sieves for several days, and distilled under reduced pressure (10−20 Torr). MeCN was distilled over P_2O_5 twice, and then distilled over CaH_2 prior to use. TEOA was distilled under reduced pressure (<1 Torr). Distilled DMA and TEOA were kept under Ar prior to use. The H_2O used in this work was distilled and deionized.

Synthesis of C_3N_4. A carbon nitride sample was synthesized according to the method reported by Antonietti et al.[63] First, cyanamide (>98%, Sigma-Aldrich Co.) was dissolved in a colloidal suspension containing 12 or 7 nm SiO_2 nanoparticles (40 wt % in water, Ludox HS-40 or SM-30, Aldrich). The ratio of SiO_2 to cyanamide was 1:1 (w/w). After the mixture was stirred at 333 K overnight, the resulting transparent mixture was heated at a rate of 2.3 K min^{-1} over 4 h to a temperature of 823 K, and this temperature was maintained for 4 h. The resulting brown-yellow powder was treated with aqueous NH_4HF_2 (4 M) solution purchased from Sigma-Aldrich Co. (>95.0%) for 24 h to remove the silica template. Handling NH_4HF_2 requires special care due to its hazardous nature. The powder was collected by centrifugation, followed by washing with distilled water three times and twice with ethanol. Finally, the powder was dried at 343 K under vacuum overnight. For comparison, bulk nonporous graphitic carbon nitride was prepared in a similar manner without a SiO_2 template.

Modification of C_3N_4 with Metal Nanoparticles. The C_3N_4 prepared was modified with metal nanoparticles by impregnation with $AgNO_3$ (99.8%, Kanto Chemicals Co.), $Cu(NO_3)_2·3H_2O$ (>99.0%, Sigma-Aldrich Co.), $H_2PtCl_6·6H_2O$ (>99.0%, Kanto Chemicals Co.), and $HAuCl_4·4H_2O$ (>99.0%, Kanto Chemicals Co.) as precursors. A total of 100 mg of C_3N_4 was dispersed in 10 mL of H_2O, followed by addition of an aqueous metal solution. The solution was distilled under reduced pressure to remove H_2O. The resulting solid sample was heated under a H_2 stream (20 mL min^{-1}) at 473 K for 1 h.

Adsorption of Ru(II) Complexes onto Metal-Loaded C_3N_4. The metal-modified materials (50 mg) were dispersed in an acetonitrile solution (25 mL) of **RuRu′** or **Ru(PS)**. When **RuP** or **Ru(Cat)** was employed, methanol was used as the solvent. The suspension was stirred at room temperature in darkness overnight to allow for adsorption/desorption equilibrium. The powder obtained was collected by filtration and washed with acetonitrile or methanol. The filtrates were collected and concentrated to 25 mL. The amount of adsorbed ruthenium complex was calculated using the following equation:

$$\text{adsorbed amount (mol g}^{-1}) = \frac{A_{before} - A_{after}}{A_{before}} \frac{C\ (\text{mol L}^{-1}) \times (25 \times 10^{-3}\ \text{L})}{50 \times 10^{-3}\ \text{g}}$$

where A_{before} and A_{after} are the absorbances of the Ru complex employed before and after the adsorption procedure, respectively, and C is initial concentration of the complex.

Material Characterization. The materials prepared were characterized by X-ray diffraction (XRD) (MiniFlex600, Rigaku; Cu Kα radiation), UV−vis diffuse reflectance spectroscopy (DRS) (V-565, Jasco), Fourier-transform infrared (FT-IR) spectroscopy (FT-IR-610, Jasco), X-ray photoelectron spectroscopy (XPS) (ESCA-3400, Shimadzu), and transmission electron microscopy (TEM) (JEM-2010F, JEOL). The binding energies determined by XPS were corrected by using the C 1s peak (285.0 eV) as a reference. The Brunauer−Emmett−Teller (BET) surface area was measured using a BELSOEP-mini II instrument (BEL Japan) at liquid nitrogen temperature.

Emission Decay Measurements. Emission decay profiles were acquired via the single photon counting method, using a FluoroCube spectrometer [Emission Decay; excitation light source, nanoLED-440 (λ_{ex} = 444 nm); detector, TBX-04, Horiba (λ_{ob} = 700 nm); cutoff filter, R60]. The spectra were recorded at room temperature using a DMA solution (4.0 mL) containing a solid sample (3.0 mg) adsorbed with **Ru(PS)** (3.4 μmol g^{-1}). The suspension was bubbled with argon gas for 20 min prior to the measurement.

Time-Resolved IR Absorption Measurements. Measurements were obtained using a homemade spectrometer described previously.[49,50] Powders of C_3N_4 and Ag/C_3N_4 were applied to a CaF_2 plate at a density of 1.5 mg cm^{-2} and placed into an IR cell for measurements. The samples were photoexcited using a 355 nm UV pulse from an Nd:YAG laser (Continuum Surelite I; duration, 6 ns; power, 0.5 mJ; repetition rate, 5−0.1 Hz), and transient absorptions in the visible to mid-IR region were measured in vacuum. The time resolution of this spectrometer was limited to 1−2 μs by the bandwidth of the amplifier (Stanford Research Systems, SR560, 1 MHz).

Photocatalytic Reaction. Reactions were performed at room temperature using an 8 mL test tube that contained 4 mL of solution and 4 mg of photocatalyst powder. For reactions in water, ethylenediaminetetraacetic acid disodium salt dihydrate (EDTA·2Na; 99.0%, Kanto Chemicals Co.), sodium ascorbate (99.9%, Kanto Chemicals Co.), or potassium oxalate monohydrate ($K_2C_2O_4·H_2O$; 99.0%, Kanto Chemicals Co.) was used as the electron donor as a 10 mM aqueous solution. Prior to irradiation, the suspension was purged with CO_2 (Taiyo Nippon Sanso Co., >99.995%) for 20 min. A 400 W high-pressure Hg lamp (SEN) was employed as a light source, in combination with an aqueous $NaNO_2$ solution to allow for visible light irradiation (λ > 400 nm), unless otherwise stated. The gaseous reaction products were analyzed using a gas chromatograph with a thermal conductivity detector (TCD) (GL Science, model GC323), an

DOI: 10.1021/jacs.6b01997
J. Am. Chem. Soc. 2016, 138, 5159−5170

activated carbon column, and argon carrier gas. The HCOOH generated in the liquid phase was analyzed using a capillary electrophoresis system (Otsuka Electronics Co., model CAPI-3300). As a control, a blank experiment was conducted in a similar manner but without irradiation. In this work, selectivity for HCOOH during the CO_2 reduction reaction was calculated on the basis of the ratio of HCOOH generated to the total amount of reduction products (i.e., HCOOH, CO, and H_2).

Apparent quantum yields (AQYs) for HCOOH production were determined using a 300 W xenon lamp (Asahi Spectra, MAX-303) fitted with a band-pass filter in the same manner reported previously.[24,26] AQYs were estimated by the equation

$$\text{AQY}\ (\%) = AR/I \times 100$$

where R and I represent the rates of HCOOH production and incident photons, respectively. A indicates the coefficient of reactions: $A = 2$ for **RuP**/C_3N_4 and $A = 4$ for **RuRu′**/Ag/C_3N_4. The total number of incident photons (10 mW) was measured using a spectroradiometer (Eko Instruments, LS-100).

Isotope-Tracer Experiments. $^{13}CO_2$ (^{13}C, 99%) was purchased from Aldrich Co. No contamination of $H^{13}COOH$ in the $^{13}CO_2$ gas was detected using ^1H NMR spectroscopy. The $^{13}CO_2$ gas was introduced into a DMA/TEOA mixed solution (4:1 (v/v), 2.0 mL) or an aqueous EDTA·2Na solution (10 mM, 2 mL) containing 4.0 mg of the photocatalyst powder, after degassing the solution was degassed by freeze–pump–thaw cycling. The no-deuterium proton NMR (No-D NMR) spectra for reaction solutions were obtained using a JEOL JNM-ECA 400 spectrometer. Solids were removed before measurements by filtration.

■ ASSOCIATED CONTENT

Supporting Information

The Supporting Information is available free of charge on the ACS Publications website at DOI: 10.1021/jacs.6b01997.

Additional characterization and reaction data, including FT-IR spectra of **RuRu′**/C_3N_4, **RuRu′**, and unmodified C_3N_4, No-D NMR spectra of a reacted solution using Ag/C_3N_4, XPS spectra of Ag/C_3N_4, UV–vis diffuse reflectance spectra of **RuRu′**/Ag/C_3N_4, XRD patterns, FT-IR spectra, UV–vis diffuse reflectance spectra, XPS spectra of **RuRu′**/Ag/C_3N_4 before and after reaction, time courses of CO_2 reduction in a mixed solution of DMA and TEOA using **RuRu′**/Ag/C_3N_4 with different **RuRu′** amounts and in aqueous potassium oxalate solution using **RuRu′**/Ag/C_3N_4, and results of CO_2 reduction reaction in a mixed solution of DMA and TEOA using **RuRu′**/Ag/C_3N_4 under different irradiation wavelengths (PDF)

■ AUTHOR INFORMATION

Corresponding Authors

*ishitani@chem.titech.ac.jp

*maedak@chem.titech.ac.jp

Notes

The authors declare no competing financial interest.

■ ACKNOWLEDGMENTS

We acknowledge the Noguchi Institute, the Murata Science Foundation, the PRESTO/JST program "Chemical Conversion of Light Energy", and a Grant-in-Aid for Young Scientists (A) (Project No. 25709078) as well as for Scientific Research on Innovative Areas (Project No. 25107512; AnApple) for funding support. This work was also partially supported by the Photon and Quantum Basic Research Coordinated Development Program (MEXT, Japan) and a CREST program (JST).

■ REFERENCES

(1) Tanaka, R.; Yamashita, M.; Nozaki, K. *J. Am. Chem. Soc.* **2009**, *131*, 14168–14169.

(2) Langer, R.; Diskin-Posner, Y.; Leitus, G.; Shimon, L. J. W.; Ben-David, Y.; Milstein, D. *Angew. Chem., Int. Ed.* **2011**, *50*, 9948–9952.

(3) Sasano, K.; Takaya, J.; Iwasawa, N. *J. Am. Chem. Soc.* **2013**, *135*, 10954–10957.

(4) Graciani, J.; Mudiyanselage, K.; Xu, F.; Baber, A. E.; Evans, J.; Senanayake, S. D.; Stacchiola, D. J.; Liu, P.; Hrbek, J.; Sanz, J. F.; Rodriguez, J. A. *Science* **2014**, *345*, 546–550.

(5) Ishida, H.; Tanaka, K.; Tanaka, T. *Organometallics* **1987**, *6*, 181–186.

(6) Hori, Y.; Wakebe, H.; Tsukamoto, T.; Koga, O. *Electrochim. Acta* **1994**, *39*, 1833–1839.

(7) Machan, C. W.; Chabolla, S. A.; Yin, J.; Gilson, M. K.; Tezcan, F. A.; Kubiak, C. P. *J. Am. Chem. Soc.* **2014**, *136*, 14598–14607.

(8) Li, C. W.; Ciston, J.; Kanan, M. W. *Nature* **2014**, *508*, 504–507.

(9) Sato, S.; Arai, T.; Morikawa, T.; Uemura, K.; Suzuki, T. M.; Tanaka, H.; Kajino, T. *J. Am. Chem. Soc.* **2011**, *133*, 15240–15243.

(10) Arai, T.; Sato, S.; Morikawa, T. *Energy Environ. Sci.* **2015**, *8*, 1998–2002.

(11) Kang, U.; Choi, S. K.; Ham, D. J.; Ji, S. M.; Choi, W.; Han, D. S.; Abdel-Wahab, A.; Park, H. *Energy Environ. Sci.* **2015**, *8*, 2638–2643.

(12) Liu, C.; Gallagher, J. J.; Sakimoto, K. K.; Nichols, E. M.; Chang, C. J.; Chang, M. C. Y.; Yang, P. *Nano Lett.* **2015**, *15*, 3634–3639.

(13) Hawecker, J.; Lehn, J. M.; Ziessel, R. *J. Chem. Soc., Chem. Commun.* **1983**, 536–538.

(14) Takeda, H.; Koike, K.; Inoue, H.; Ishitani, O. *J. Am. Chem. Soc.* **2008**, *130*, 2023–2031.

(15) Tamaki, Y.; Koike, K.; Morimoto, T.; Ishitani, O. *J. Catal.* **2013**, *304*, 22–28.

(16) Tamaki, Y.; Koike, K.; Ishitani, O. *Chem. Sci.* **2015**, *6*, 7213–7221.

(17) Agarwal, J.; Fujita, E.; Schaefer, H. F., III; Muckerman, J. T. *J. Am. Chem. Soc.* **2012**, *134*, 5180–5186.

(18) Kuramochi, Y.; Kamiya, M.; Ishida, H. *Inorg. Chem.* **2014**, *53*, 3326–3332.

(19) Kuramochi, Y.; Itabashi, J.; Fukaya, K.; Enomoto, A.; Yoshida, M.; Ishida, H. *Chem. Sci.* **2015**, *6*, 3063–3074.

(20) Iizuka, K.; Wato, T.; Miseki, Y.; Saito, K.; Kudo, A. *J. Am. Chem. Soc.* **2011**, *133*, 20863–20868.

(21) Teramura, K.; Iguchi, S.; Mizuno, Y.; Shishido, T.; Tanaka, T. *Angew. Chem., Int. Ed.* **2012**, *51*, 8008–8011.

(22) Teramura, K.; Wang, Z.; Hosokawa, S.; Sakata, Y.; Tanaka, T. *Chem. - Eur. J.* **2014**, *20*, 9906–9909.

(23) Sato, S.; Morikawa, T.; Saeki, S.; Kajino, T.; Motohiro, T. *Angew. Chem., Int. Ed.* **2010**, *49*, 5101–5105.

(24) Maeda, K.; Sekizawa, K.; Ishitani, O. *Chem. Commun.* **2013**, *49*, 10127–10129.

(25) Maeda, K.; Kuriki, R.; Zhang, M.; Wang, X.; Ishitani, O. *J. Mater. Chem. A* **2014**, *2*, 15146–15151.

(26) Kuriki, R.; Sekizawa, K.; Ishitani, O.; Maeda, K. *Angew. Chem., Int. Ed.* **2015**, *54*, 2406–2409.

(27) Maeda, K.; Kuriki, R.; Ishitani, O. *Chem. Lett.* **2016**, *45*, 182–184.

(28) Kuriki, R.; Ishitani, O.; Maeda, K. *ACS Appl. Mater. Interfaces* **2016**, *8*, 6011–6018.

(29) Hong, J.; Zhang, W.; Wang, Y.; Zhou, T.; Xu, R. *ChemCatChem* **2014**, *6*, 2315–2321.

(30) Wang, S.; Yao, W.; Lin, J.; Ding, Z.; Wang, X. *Angew. Chem., Int. Ed.* **2014**, *53*, 1034–1038.

(31) Wang, S.; Lin, J.; Wang, X. *Phys. Chem. Chem. Phys.* **2014**, *16*, 14656–14660.

(32) Kim, W.; Yuan, G.; McClure, B. A.; Frei, H. *J. Am. Chem. Soc.* **2014**, *136*, 11034–11042.

(33) Sekizawa, K.; Maeda, K.; Koike, K.; Domen, K.; Ishitani, O. *J. Am. Chem. Soc.* **2013**, *135*, 4596–4599.

(34) Yoshitomi, F.; Sekizawa, K.; Maeda, K.; Ishitani, O. *ACS Appl. Mater. Interfaces* **2015**, *7*, 13092–13097.

DOI: 10.1021/jacs.6b01997
J. Am. Chem. Soc. 2016, 138, 5159–5170

(35) Chueh, W. C.; Falter, C.; Abbott, M.; Scipio, D.; Furler, P.; Haile, S. M.; Steinfeld, A. *Science* **2010**, *330*, 1797−1801.
(36) Maeda, K.; Domen, K. *J. Phys. Chem. Lett.* **2010**, *1*, 2655−2661.
(37) Hitoki, G.; Takata, T.; Kondo, J. N.; Hara, M.; Kobayashi, H.; Domen, K. *Chem. Commun.* **2002**, 1698−1699.
(38) Hitoki, G.; Ishikawa, A.; Takata, T.; Kondo, J. N.; Hara, M.; Domen, K. *Chem. Lett.* **2002**, *31*, 736−737.
(39) Maeda, K.; Teramura, K.; Lu, D.; Takata, T.; Saito, N.; Inoue, Y.; Domen, K. *Nature* **2006**, *440*, 295.
(40) Zhang, F.; Yamakata, A.; Maeda, K.; Moriya, Y.; Takata, T.; Kubota, J.; Teshima, K.; Oishi, S.; Domen, K. *J. Am. Chem. Soc.* **2012**, *134*, 8348−8351.
(41) Hull, J. F.; Himeda, Y.; Wang, W.-H.; Hashiguchi, B.; Periana, R.; Szalda, D. J.; Muckerman, J. T.; Fujita, E. *Nat. Chem.* **2012**, *4*, 383−388.
(42) Martindale, B. C. M.; Hutton, G. A. M.; Caputo, C. A.; Reisner, R. *J. Am. Chem. Soc.* **2015**, *137*, 6018−6025.
(43) Hashimoto, K.; Hiramoto, M.; Sakata, T.; Muraki, H.; Takemura, H.; Fujihira, M. *J. Phys. Chem.* **1987**, *91*, 6198−6203.
(44) Maeda, K.; Oshima, T.; Ishitani, O. *Phys. Chem. Chem. Phys.* **2015**, *17*, 17962−17966.
(45) When we measured unmodified C_3N_4, emission (observed at 700 nm) decayed very quickly within a few nanoseconds, even though C_3N_4 does not give an emission band at 700 nm. We think that this is because of light scattering by the C_3N_4 suspension. We could not exclude this light scattering effect completely, even after various modifications in the measurement conditions by changing the excitation and/or monitoring wavelength.
(46) Asbury, J. B.; Hao, E.; Wang, Y. Q.; Ghosh, H. N.; Lian, T. Q. *J. Phys. Chem. B* **2001**, *105*, 4545−4557.
(47) Asbury, J. B.; Hao, E.; Wang, Y. Q.; Lian, T. Q. *J. Phys. Chem. B* **2000**, *104*, 11957−11964.
(48) Thomas, A.; Fischer, A.; Goettmann, F.; Antonietti, M.; Müller, J.-O.; Schlögl, R.; Carlsson, J. M. *J. Mater. Chem.* **2008**, *18*, 4893−4908.
(49) Yamakata, A.; Ishibashi, T.; Onishi, H. *J. Phys. Chem. B* **2001**, *105*, 7258−7262.
(50) Yamakata, A.; Yoshida, M.; Kubota, J.; Osawa, M.; Domen, K. *J. Am. Chem. Soc.* **2011**, *133*, 11351−11357.
(51) Yamakata, A.; Yeilin, H.; Kawaguchi, M.; Hisatomi, T.; Kubota, J.; Sakata, Y.; Domen, K. *J. Photochem. Photobiol., A* **2015**, *313*, 168−175.
(52) Furuhashi, K.; Jia, Q.; Kudo, A.; Onishi, H. *J. Phys. Chem. C* **2013**, *117*, 19101−19106.
(53) Yamakata, A.; Vequizo, J. J. M.; Kawaguchi, M. *J. Phys. Chem. C* **2015**, *119*, 1880−1885.
(54) Yamakata, A.; Vequizo, J. J. M.; Matsunaga, H. *J. Phys. Chem. C* **2015**, *119*, 24538−24545.
(55) Wang, X.; Maeda, K.; Thomas, A.; Takanabe, K.; Xin, G.; Carlsson, J. M.; Domen, K.; Antonietti, M. *Nat. Mater.* **2009**, *8*, 76−80.
(56) Yamada, Y.; Nomura, A.; Tadokoro, H.; Fukuzumi, S. *Catal. Sci. Technol.* **2015**, *5*, 428−437.
(57) Maeda, K.; Wang, X.; Nishihara, Y.; Lu, D.; Antonietti, M.; Domen, K. *J. Phys. Chem. C* **2009**, *113*, 4940−4947.
(58) Zhang, G.; Zang, S.; Wang, X. *ACS Catal.* **2015**, *5*, 941−947.
(59) Zhang, G.; Lan, Z. -A.; Lin, L.; Lin, S.; Wang, X. *Chem. Sci.* **2016**, DOI: 10.1039/c5sc04572j.
(60) Zheng, Y.; Lin, L.; Wang, B.; Wang, X. *Angew. Chem., Int. Ed.* **2015**, *54*, 12868−12884.
(61) Yin, S.; Han, J.; Zhou, T.; Xu, R. *Catal. Sci. Technol.* **2015**, *5*, 5048−5061.
(62) Zhang, J.; Chen, Y.; Wang, X. *Energy Environ. Sci.* **2015**, *8*, 3092−3108.
(63) Goettmann, F.; Fischer, A.; Antonietti, M.; Thomas, A. *Angew. Chem., Int. Ed.* **2006**, *45*, 4467−4471.

DOI: 10.1021/jacs.6b01997
J. Am. Chem. Soc. 2016, 138, 5159−5170